Two-dimensional silicon boride on $ZrB_2(0001)$

Takashi Aizawa,* Shigeru Suehara, and Shigeki Otani
National Institute for Materials Science, 1-1 Namiki, Tsukuba, Ibaraki 305-0044, Japan

(Received 9 November 2018; published 24 January 2019)

A two-dimensional silicon boride phase, "siliborophene," was formed on a $ZrB_2(0001)$ single-crystal surface, which coincided with the 2×2 periodicity of the substrate. The phonon dispersion relations were measured using high-resolution electron energy-loss spectroscopy and were compared with theoretical predictions based on first-principles density functional theory. Among many theoretically derived surface models, only one structure made of Si_3B_6 can reproduce details of the measured phonon dispersion. That model consists of a cyclic boron ring (cB_6) capped by a Si atom, SiB_6 group, and sp^2-like Si atoms connecting them. This structure is much more robust than that of silicene: it shows no order–disorder transition until 1300 K; above that temperature, Si is desorbed gradually. Electron band calculation of the isolated film of Si_3B_6 displays a band crossing at the $\overline{K}$ point, which makes this material promising for use with Fermi-level engineering.

DOI: 10.1103/PhysRevMaterials.3.014005

I. INTRODUCTION

Two-dimensional (2D) materials such as graphene have become an important trend during this century [1]. Actually, 2D materials of many kinds have been identified and explored extensively to the present day [2]. We pioneered graphene phonon measurements in the early 1990s. The phonon dispersion relation of graphene, which was originally useful to clarify the monoatomic thickness and the interaction between graphene and the substrate [3], is still used today [4].

Recently, silicene (2D honeycomb lattice of silicon) on ZrC(111) [5] and $ZrB_2(0001)$ [6] has been fabricated by depositing atomic Si. The phonon dispersions of the material have been studied. We used transition-metal carbide (TMC) [7] or diboride (TMB_2) [8] substrates because of their robustness, high melting point, and chemical stability. Regarding metal atoms, almost all interstitial sites have already been occupied by C or B atoms, which is expected to cause less diffusivity of surface-deposited atoms into bulk than on pure metal substrates. On both substrates, the $(\sqrt{3} \times \sqrt{3})$ silicene coincides with the (2×2) metal-terminated substrate. The measured phonon dispersions were compared with the first-principles calculation, which yielded fruitful information related to the atomic structure. The silicene layers exhibit an order-disorder transition: $2 \times 2 \leftrightarrow 1 \times 1$ transition is observed in reflection high-energy electron diffraction (RHEED) at low temperatures [1000 K on ZrC(111) and 870 K on $ZrB_2(0001)$]. On $ZrB_2(0001)$, the silicene lattice constant is 366 pm, which is fairly small compared with the theoretically predicted lattice constant (383–389 pm) for a free-standing silicene [9–11]. Probably the large interaction between the silicene and the substrate produces compressive stress in the silicene layer. In contrast, the silicene lattice constant of the well-known Ag(111)4×4-Si phase is 385 pm, which is very close to the predicted value.

Fleurence *et al.* discovered spontaneous formation of silicene upon heating a thin-film $ZrB_2(0001)$ epitaxial layer grown on Si(111) [12,13], which spurred many studies using x-ray photoelectron spectroscopy (XPS) [14], scanning tunneling microscopy (STM), and theoretical calculation [15]. Although the silicene layer is oxidized in air, it is readily recovered upon heating in a vacuum. This phenomenon suggests high mobility of Si on and in the $ZrB_2(0001)$ thin film. For electronic device applications, several protective layers against air exposure have been examined, but such layers are not yet successful [16–18].

Regarding 2D boron, "borophene," several groups have reported formation on Ag(111) [19,20], although it was not a honeycomb lattice similar to graphene. The electronic structure was clarified as metallic [21]. Recently, honeycomb borophene was reported on an Al(111) substrate with a large charge transfer [22]. However, the graphenelike honeycomb boron layer (B-layer termination) is known to exist on the group-5 or -6 $TMB_2(0001)$ surfaces such as $NbB_2(0001)$ [23], $TaB_2(0001)$ [24], and $WB_2(0001)$ [25]. Group-4 $TMB_2(0001)$ (TM = Ti, Zr, Hf) are usually terminated with a metal atom layer after heat-cleaning in a vacuum. When boron is deposited on the $ZrB_2(0001)$ metal-terminated surface, boron forms a $\sqrt{3} \times \sqrt{3}$ honeycomb borophene layer [26] in which one B adatom exists in every $\sqrt{3} \times \sqrt{3}$ unit cell [27].

In this work, we explored a 2D silicon-boron compound on $ZrB_2(0001)$, a well understood substrate for B or Si adsorption. The compressive stress in the silicene layer can be released if some Si atoms in silicene are replaced by B. In the literature, several theoretical works are found for 2D Si-B systems. They considered Si_3B analogously with BC_3 [28,29]

*aizawa.takashi@nims.go.jp

and hBN-type SiB [30]. At first, we expected such a phase to be formed, but the formation does not occur, at least on this substrate.

II. METHODS

A. Experiment

The experiment was performed using a high-resolution electron energy-loss spectroscopy (HREELS) system combined with a sample preparation chamber. The mu-metal (PC-grade permalloy) HREELS chamber achieves both good magnetic shielding and extremely high vacuum performance. It is evacuated using a 400-ℓ/s ion pump and a nonevaporable getter pump (2000 ℓ/s), which achieve base pressure of less than 2×10^{-9} Pa at room temperature (RT) of 25 °C. The spectrometer (Delta-0.5; SPECS GmbH), which has a double-pass cylindrical electrostatic electron monochromator and a single-pass analyzer, was tuned in this experiment to energy resolution of about 1.5 meV in full width at half maximum to provide a good signal-to-noise ratio. The electron incidence angle θ_{in} was fixed at 75° from surface normal. The detection angle θ_{out} was varied to change the excited phonon wave vector parallel to the surface [31]. A back-view low-energy electron-diffraction system (BDL800-MCP; OCI Vacuum Microengineering Inc.) was used with this chamber to adjust the sample azimuth.

The sample preparation chamber, a conventional stainless-steel ultra-high vacuum (UHV) chamber, was pumped with 250-ℓ/s turbomolecular and Ti sublimation pumps, the base pressure of which was less than 2×10^{-8} Pa. The apparatus included the following components: a RHEED system for checking the surface periodicity and ordering, a cylindrical mirror electron analyzer for Auger electron spectroscopy (AES) to check the surface chemical composition, an electron-beam evaporator (EFM 3; Scienta Omicron GmbH), an ion gun (IQE 11/35; SPECS GmbH) for sputter cleaning of the sample surface, and a small load-lock system for sample exchange. Silicon was evaporated from a direct-current-heated (about 1500 K) retractable Si wafer (25 mm × 4 mm × 0.4 mm) placed 20–30 mm distant from the substrate surface. Boron was evaporated from a β-boron rod using the EFM 3 evaporator. A sample can be heated using electron bombardment (1–1.5 keV, 5–200 mA) on the sample's back. The temperature was measured using infrared (2.0 μm, $\epsilon = 0.4$) and two-color (0.85 μm/1.00 μm) optical pyrometers. All AES, RHEED, and HREELS data were taken at RT.

A ZrB_2 single-crystal rod was grown in our laboratory using rf-heated floating zone method [32]. The (0001) substrates (10 × 8 mm^2 and 1 mm thick) were cut from it after aligning the [0001] direction using an x-ray back Laue method with accuracy of ±1°. One face of the (0001) surface was polished to a mirror finish with diamond paste (2 μm). The polished substrate was cleaned ultrasonically with acetone before introduction into a vacuum. The substrate was degassed at about 1500 K in the UHV. It was finally cleaned by heating several times briefly at temperatures higher than 2500 K. The clean surface exhibited a clear 1 × 1 RHEED pattern with low background, with impurities such as C or O only slightly detected in the AES.

B. Calculation

All first-principles calculations, including simulated annealing molecular dynamics (SAMD) for preliminarily exploring surface structures and lattice dynamics (phonons) by density functional perturbation theory (DFPT), were conducted using QUANTUM-ESPRESSO (QE) version 6 suite [33,34] except for the core-level energy calculation. The semilocal generalized gradient approximation, the Perdew-Burke-Ernzerhof (PBE) exchange-correlation functional [35], and the PBE ultrasoft pseudopotentials distributed by Rutgers University [36] were adopted for this work. Because the van der Waals (vdW) correction only slightly affected the structures, as shown in the Supplemental Material [37], no vdW correction was applied.

The substrate $ZrB_2(0001)$ model consisted of seven alternate stackings of close-packed Zr and honeycomb B layers with surface unit area of 2 × 2. The surface was modeled in a fully periodic slab construction separated by a vacuum layer larger than 1.5 nm (a so-called "supercell slab" surface model) with the preliminarily optimized lattice constants of $a = 0.6342$ nm and $c = 3.1867$ nm. The top and bottom surfaces were terminated with Zr layers according with the stable clean surface of $ZrB_2(0001)$ [23]. A Si_xB_y layer was put on one side of the $ZrB_2(0001)$ slab. A stable structure was found using SAMD calculations. The model was heated and kept at about 1200 K for 10 ps with a Berendesen thermostat [38], with subsequent cooling to room temperature in 10 ps. To make our surface structure exploration more efficient, the bottom five layers were fixed. The Si-B surface layer and the two subsurface layers of the substrate were allowed to move in SAMD. The SAMD-derived structures were screened by comparison the phonon dispersion of the DFPT calculation with the experiment. Phonon dispersion of the most plausible Si-B structure was finally re-evaluated under higher cost: the Si-B layers were put on both sides of the substrate slab; all atoms were moved fully with a higher numerical precision condition.

Basic computational parameters such as cutoff energies of plane wave and charge density (E_{cut} and E^{ρ}_{cut}), and quantities of Brillouin zone (BZ) sampling for electrons and phonons ($\boldsymbol{k}$ point and $\boldsymbol{q}$ point) were checked preliminarily in terms of numerical convergence and reproduction of the ZrB_2 bulk phonons, silicene, and borophene structures in our earlier works [5,6,27]. The SAMD calculations were done at a time step of 2 fs, which can sample >10 times of the atomic movements in the highest frequency phonon period in this system (about 30 THz). For high-throughput SAMD, $E_{\text{cut}}(E^{\rho}_{\text{cut}}) = 22$ Ry (280 Ry) was used with 2 × 2 × 1 $\boldsymbol{k}$-points BZ sampling. The maximum allowable atomic force of <0.01 mRy/a.u. was used in the post-SAMD relaxation procedure for obtaining local-minimum-energy structures. For the DFPT phonon calculations of the SAMD-derived structures, 26 Ry (280 Ry) with 4 × 4 × 1 $\boldsymbol{k}$ points and 3 × 3 × 1 $\boldsymbol{q}$ points BZ sampling were used. As for the plausible structure models, the cutoff of 40 Ry (320 Ry) and the BZ samplings of 6 × 6 × 1 $\boldsymbol{k}$ points and 6 × 6 × 1 $\boldsymbol{q}$ points were used. Gaussian smearing widths of 15 and 7.5 mRy were employed, respectively, in the screening and the final production calculation runs. As described herein, atomic structures were visualized using VMD [39] and VESTA [40] software.

III. RESULTS AND DISCUSSION

A. Experimentally obtained results

We tried several coadsorptions of B and Si on $ZrB_2(0001)$ substrate, which clarified the following. To produce a well-ordered Si_xB_y surface phase, precise control of the B coverage is necessary. Controlled removal of the adsorbed B by heat treatment is difficult because the necessary temperature is too high: more than 2200 K. Therefore, the B amount should be controlled at deposition. On the other hand, Si can be desorbed more easily at around 1200–1300 K. Once the Si-B ordered phase is formed, the sticking probability of Si is reduced considerably: it readily reaches saturation. Based on these facts, we used a recipe to produce a well-ordered Si-B overlayer as explained below.

(1) The $ZrB_2(0001)$ is first cleaned by flash heating at >2300 K in UHV.

(2) After 7–10-min cooling, Si is deposited to make $ZrB_2(0001)2 \times 2$ silicene under RHEED monitoring.

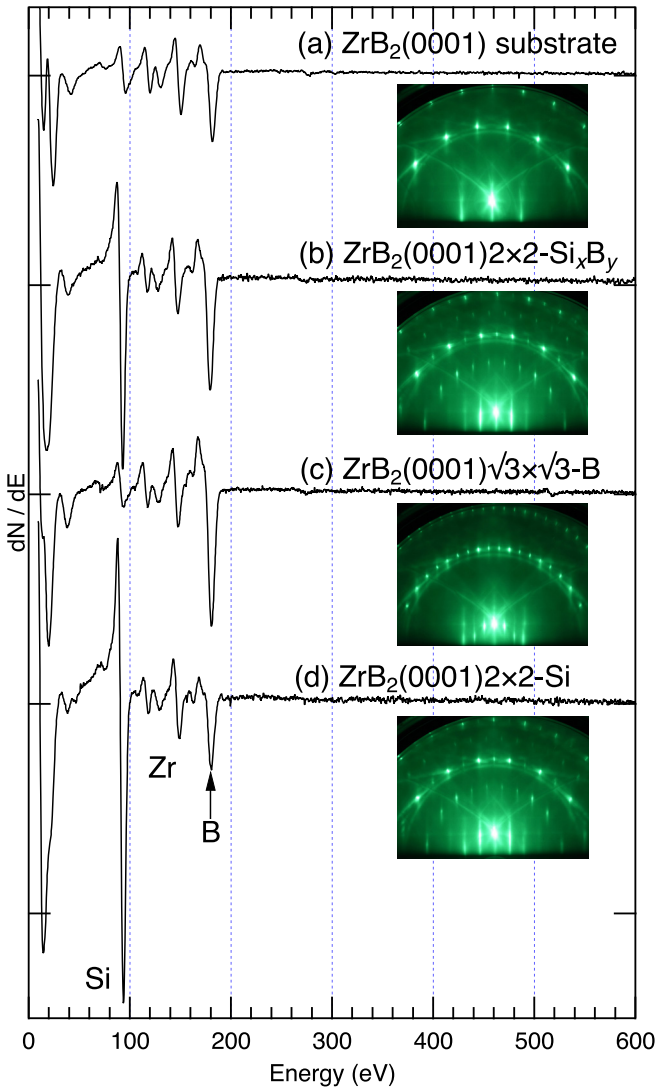

FIG. 1. AES spectra for (a) clean $ZrB_2(0001)$, (b) 2×2-Si_xB_y, (c) $\sqrt{3} \times \sqrt{3}$-B, and (d) 2×2-silicene 2D phases. Insets show the respective RHEED patterns ($E_0 = 15$ keV, $\langle 10\bar{1}0 \rangle$ azimuth).

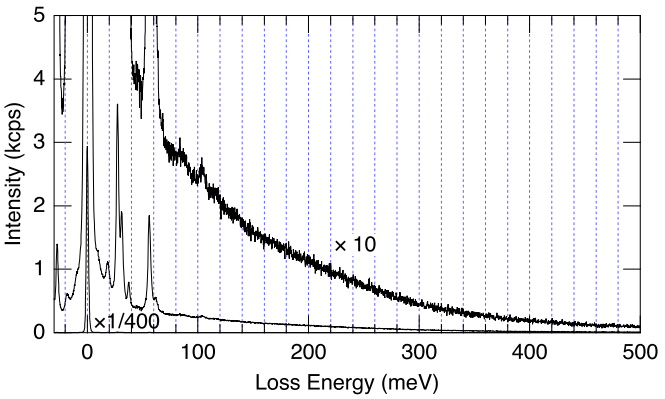

FIG. 2. Wide-energy-range specular HREEL spectrum for $ZrB_2(0001)2 \times 2$-Si_xB_y. $E_0 = 2.0$ eV.

(3) The sample is heated to 1200 K, where the 2×2 ordering disappears in RHEED (disordered 1×1 phase).

(4) B is deposited on this surface at 1200 K under RHEED monitoring. The 2×2 diffraction spots appear again. The B deposition is stopped just when the 2×2 pattern becomes clearest. In Fig. 1, the AES and RHEED of the above-prepared $ZrB_2(0001)2 \times 2$-Si_xB_y (b) are compared with (a) clean, (c) borophene-covered, and (d) silicene-covered $ZrB_2(0001)$, where each AES spectrum is normalized with one of Zr MVV peaks at 150 eV. The Si intensity of (b) is less than that of (d); also, the B intensity of (b) is less than that of (c), suggesting formation of a different monolayer 2D Si-B compound. From AES results, the coverage of B in the sample (b) can be estimated roughly at 1.4 monolayers [ML: one atom per unit cell of the substrate $ZrB_2(0001)$], based on the structure model for $\sqrt{3} \times \sqrt{3}$-B phase, in which the B coverage is 7/3 ML [27]. The Si coverage can be estimated similarly at 0.8 ML based on the silicene 2×2 structure (6/4 ML) [12].

The 2D silicene shows an order-disorder transition (melting) at low temperatures: 870 K on $ZrB_2(0001)$ [6] and 1000 K on ZrC(111) [5]. The 2×2-Si_xB_y layer showed no order-disorder transition up to 1300 K. At temperatures higher than 1300 K, Si evaporated gradually; the 2×2 structure was lost in several minutes. Subsequently however, additional Si deposition at 1200 K recovered the 2×2 structure. The Si coverage seems saturated at 1200 K: The Si intensity in AES was increased only slightly after the 2×2 structure was completed. Probably, the sticking probability of Si decreases drastically after the 2×2-Si_xB_y layer is completed. These results suggest that the 2×2-Si_xB_y layer is much stabler than the silicene layer.

The prepared $ZrB_2(0001)2 \times 2$-Si_xB_y was the subject of the HREELS measurement. Figure 2 exhibits a wide-energy-range specular HREELS. No loss peak appears above 150 meV: no contamination-related (C-O, C-H, or O-H) stretching vibration was detected. Several loss peaks appear at 18.3, 27.4, 31.0, 37.4, 56.1, 61.6, and 103.5 meV. These loss features are clearly different from those of silicene [6] and those of borophene [26], indicating that this layer is not a mixed phase of silicene and borophene, but that it is instead a 2D compound consisting of Si and B. We measured

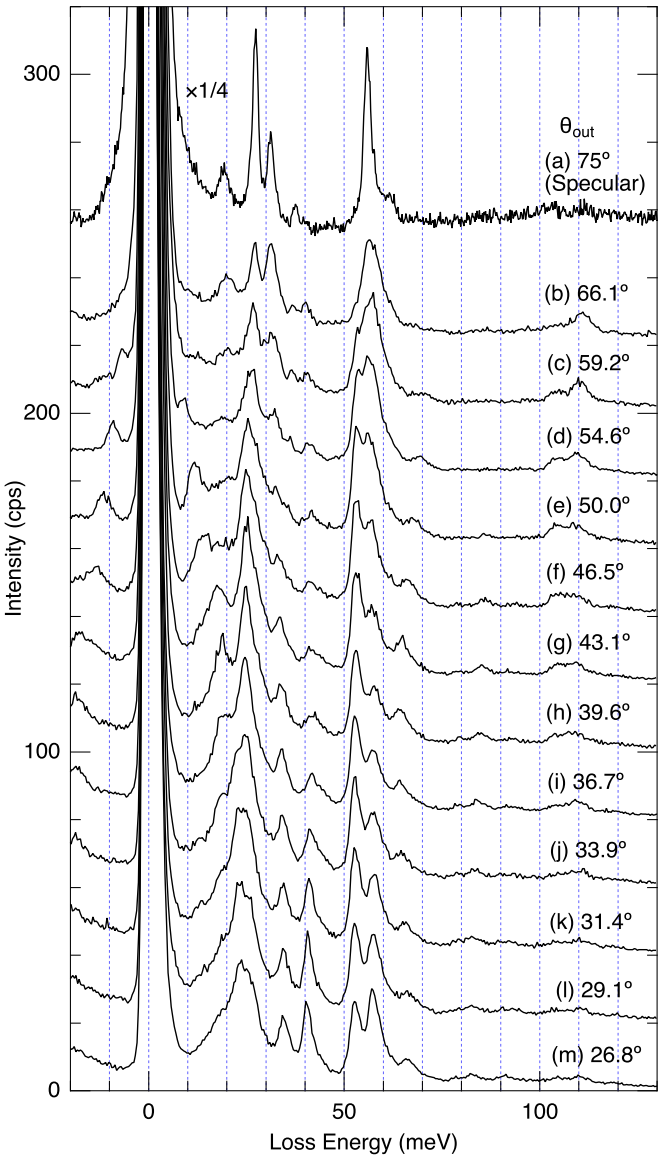

FIG. 3. Off-specular HREEL spectra for $ZrB_2(0001)2 \times 2\text{-}Si_xB_y$. $E_0 = 12.0$ eV. Azimuth is $\langle 11\bar{2}0\rangle$ ($\bar{\Gamma} - \bar{K}$). The calculated momentum transfer in $Å^{-1}$ is (a) 0, (b) 0.092, (c) 0.190, (d) 0.268, (e) 0.355, (f) 0.426, (g) 0.502, (h) 0.582, (i) 0.655, (j) 0.724, (k) 0.790, (l) 0.852, and (m) 0.915.

off-specular HREELS with three primary electron energies (E_0): 9, 12, and 15 eV. One example of a series taken at various detection angles is presented in Fig. 3. Plotting the loss peak energies versus the momentum transfer parallel to the surface yields the surface phonon dispersion relation exhibited in Fig. 4. Not all phonon modes are necessarily detected in the adopted measuring conditions.

As a clear characteristic, two high-frequency phonon modes appear at around 105 and 110 meV with little dispersion, suggesting the existence of local strong B-B covalent bonds. These frequencies are higher than the B-B stretching in ZrB_2 bulk (<100 meV) or the highest-frequency mode in the borophene layer on the (0001) surface [27]. In the next section, the atomic structure of the Si_xB_y layer is inferred from

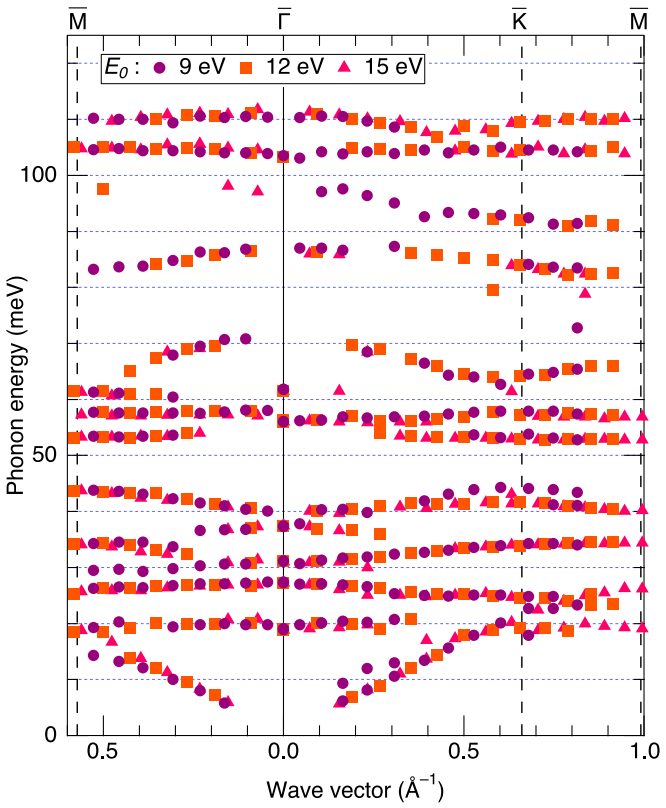

FIG. 4. Measured phonon dispersion for $ZrB_2(0001)\,2 \times 2\text{-}Si_xB_y$.

measured phonon dispersion relations using first-principles calculations.

B. Theoretical analysis

First, the SAMD calculations were applied to obtain a tentative structure having a local-minimum energy in a given composition. In some cases, the SAMD calculation reached different structures of the same composition from various initial structures. In the next step, phonon dispersions of the obtained structures were calculated and compared with the experiment to judge the structure. The first criterion is whether or not the characteristic high-frequency modes (105 and 110 meV) were well reproduced. Because large experimental errors can be contained in the AES coverage estimation, we tried fairly wide Si:B compositional ranges. Figure 5 presents examples.

The silicene structure and its phonon dispersion relations [6] are well reproduced in this calculation, as shown in Fig. 5(a), except for the low-frequency region. Because some substrate atoms are fixed, the low-energy substrate phonon is evaluated insufficiently. Then some Si atoms are replaced with B, as exhibited in Figs. 5(b)–5(g). In these structures, when no B-B bond exists (b)–(d), the highest phonon frequency is less than 100 meV. Structures including B-B dimers (e), or B–B–B trimers (f) exhibit dispersionless high-frequency bands, respectively, at around 116 and 103 meV. These values closely approximate the experimentally obtained data, so that one might expect a mixed phase model of the boron dimers and trimers. However, the other phonon modes are not well fitted

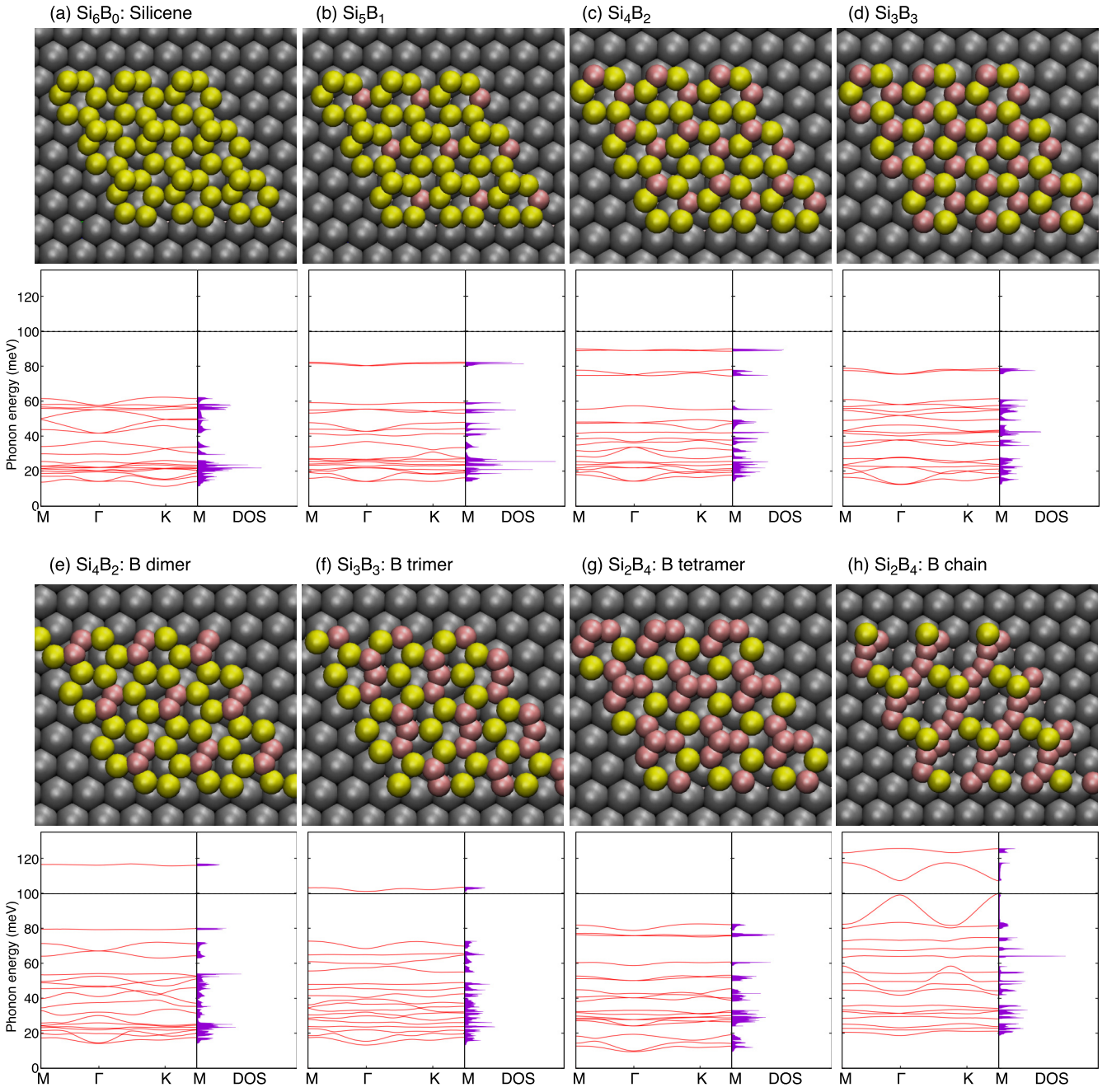

FIG. 5. Structure models and phonon dispersions. Gray, yellow, and red-brown balls respectively represent Zr, Si, and B atoms. Phonon dispersions are drawn along $\overline{M}$–$\overline{\Gamma}$–$\overline{K}$–$\overline{M}$ of the substrate (2×2) unit cell.

to the experiment. Even if the structure includes B-B bonds, the B_4 tetramer structure (g) gives the lower frequency as around 82 meV at the highest. In the case in which B makes a continuous chain, the highest frequency B-B stretching modes have fairly large dispersion, as shown in Fig. 5(h), which is inconsistent with the experiment. From these and many other SAMD results, the following can be inferred.

(i) Boron atoms are adsorbed preferably at the threefold hollow sites of the substrate.

(ii) Si prefers bridge or on-top sites rather than the hollow site.

(iii) Structures containing only Si-B bonds cannot produce the experimentally observed high-frequency dispersionless phonons.

(iv) The B-B bonds are necessary for the observed high-frequency phonons.

(v) However, structures in which one B connects to three B atoms are omitted because they give much lower frequencies.

Bearing these points in mind, in the next step, we examined structure models modified from the boron honeycomb, as in the ZrB_2 bulk. The B-B stretching phonon mode should have large dispersion as in Fig. 5(h) or in the bulk phonon of ZrB_2

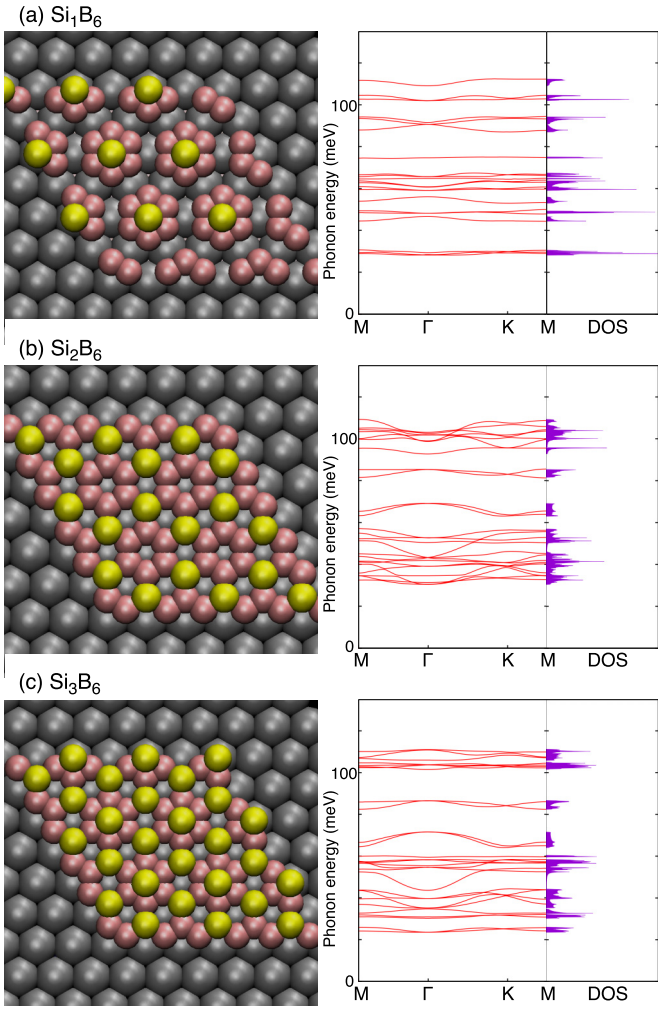

FIG. 6. Structure models containing cB_6 and their phonon dispersions. The notation is the same as that used in Fig. 5.

[23,27] if boron atoms made a continuous network through B-B covalent bonds. Therefore, we considered structure models containing an isolated cyclic B_6 (cB_6) group as a building block. Figure 6 presents results of three examined models. Model (a) consists of an isolated cB_6 capped by a Si atom (capping Si): SiB_6 in the 2×2 unit cell, similarly to molecular adsorption. In model (b), cB_6 units are mutually connected by Si atoms (bridging Si). This connection is inverse to the BSi_3 structure, which was examined theoretically [28,29]. In model (c), the SiB_6 group is connected with the bridging Si. All these models were little altered in the SAMD at 1200 K for 10 ps within the restriction of 2×2 periodicity.

The phonon dispersion relations of the model (a) are completely flat, indicating localized vibrations as in a molecule. The phonons of models (b) and (c) resemble one another. However, the high-frequency phonon bands of the model (b) show considerable dispersions in 93–110 meV, whereas those in the model (c) are rather flat (103–110 meV). Model (c) seems to fit the experimentally obtained data best. Table I presents the formation energy of these structures from the silicene and the borophene phases in the 2×2 unit cell of the substrate. The (c) Si_3B_6 "siliborophene" phase has the lowest

TABLE I. Surface formation energy of surface silicon boride per the (2×2) unit cell. The formation energies (ΔH_f)[a] were estimated roughly from total lattice energies of the respective phases: clean surface (E_0), silicene (E_{Si_6}), borophene (E_{B_9}), and siliborophene ($E_{Si_xB_y}$) on the $ZrB_2(0001)$ 2×2 area.

Surface	Si_1B_6	Si_2B_6	Si_3B_6
ΔH_f (eV/2× 2 unit cell)	2.513	−0.813	−1.517

[a] $\Delta H_f = E_{Si_xB_y} - E_0 - x(E_{Si_6} - E_0)/6 - y(E_{B_9} - E_0)/9$.

negative value among these structures. The negative (exothermic) formation energy proves the phase stability: it does not decompose spontaneously into silicene and borophene phases. In Fig. 7, the finally determined structure model of the siliborophene is presented. The B-B distance in the cB_6 group is slightly shorter than that in the boron honeycomb lattice in ZrB_2. The capping Si atom on cB_6 protrudes outward considerably. The detailed atomic coordinates used in the high-precision phonon calculation are given in the Supplemental Material [37]. The calculated phonon dispersions are shown for comparison with the experimentally obtained data in Fig. 8. One phonon branch observed experimentally between 90 and 100 meV is assignable to the optical mode of the substrate boron [23,27]. Except for this mode, all experimentally observed phonon modes are well reproduced in the siliborophene phonon calculation. Several calculated modes (e.g., a mode between 45 and 55 meV) were not observed from experimentation, probably because of the small cross section in the adopted experiment conditions. The overall agreement between the theoretical calculation and the experiment is surprising, indicating excellent credibility of this model.

Figure 9 presents the projected electronic band structure of the siliborophene layer on ZrB_2. Analyses of the electronic density of states (DOS) and band structure were conducted by projecting the wave function to each pseudoatomic orbital to represent eigenstates and then summing only for the related atoms. The spilling parameter, which is a measure of difference between preprojection and postprojection for occupied states, was 0.0022 [41]. The projected DOS of the

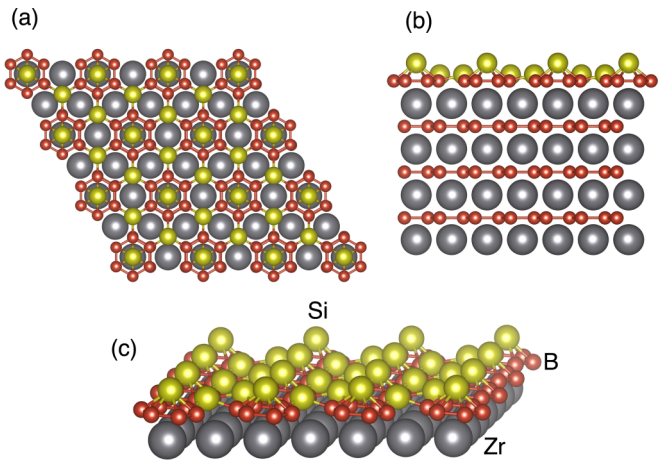

FIG. 7. Determined structure model of Si_3B_6 siliborophene: (a) top, (b) side, and (c) bird's-eye views.

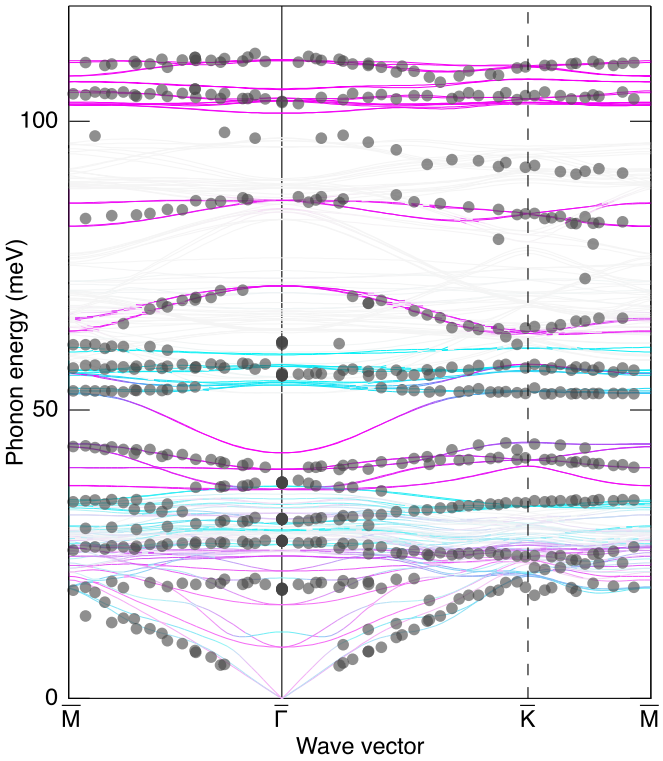

FIG. 8. Calculated phonon dispersion curves (lines) of Si_3B_6 siliborophene compared with experimentally obtained data (gray dots). The magenta and cyan colors respectively represent the partial density of states for in-plane and out-of-plane vibrations in the siliborophene layer.

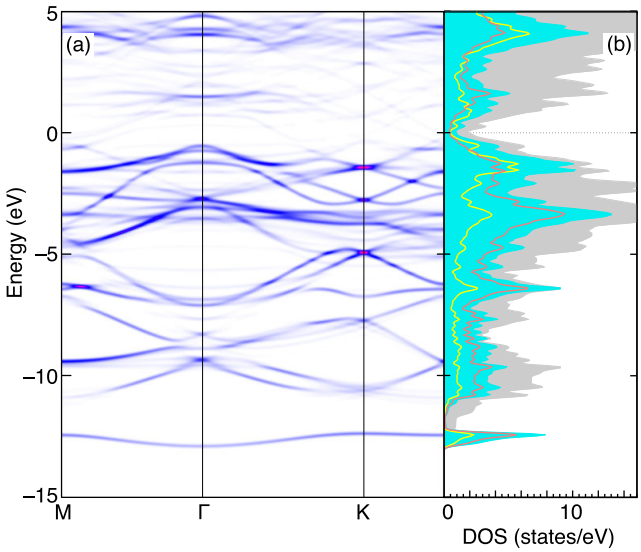

FIG. 9. Calculation results of (a) projected electronic band structures for the Si_3B_6 siliborophene layer, and (b) electronic DOS. Gray and light blue shadows represent the total slab DOS ($\times 1/2$) and the siliborophene DOS, respectively. Red and yellow lines are, respectively, boron and silicon components in the siliborophene DOS. The Fermi level (E_f) is inferred as zero electron volts.

siliborophene layer [Fig. 9(b)] shows a very small minimum around the Fermi level in contrast to other cB_6 models (not shown here), again suggesting siliborophene stability. The Löwdin charges [42] of the capping Si, bridging Si, and B in cB_6 are estimated respectively as $+0.72$, $+0.71$, and -0.35. From these values, the total charge in the siliborophene layer is expected to be almost neutral: large charge transfer is not predicted between the siliborophene layer and the ZrB_2 substrate within the Löwdin charge framework.

The core-level (initial state) energies of the siliborophene were evaluated using the projector augmented wave method (PAW) with the Vienna ab initio simulation package (VASP) [43] with cutoff energy of 550 eV in the $6 \times 6 \times 1$ $\boldsymbol{k}$-point sampling. We confirmed that the structures and eigenvalues calculated using VASP with the PBE exchange correlation were consistent with those from QE, with only a small numerical error. The $2p$ core level of the capping Si on cB_6 is lower (deeper) than the bridging Si by 1.09 eV. The B1s in the siliborophene layer is higher (shallower) than that of the center layer B in the slab (where the B atom is regarded as in the ZrB_2 bulk) by 0.55 eV. Although the total charge is almost identical between the capping and bridging silicon, the core level differs by about 1 eV. Probably the charge redistribution between Si3s and Si3p causes the core-level shift. Such noncovariant behavior between the atomic charge and the core-level shift has been observed in the B1s surface core-level shift on NbB_2(0001) [44]. The electronic structures must be confirmed experimentally in future studies using high-resolution photoelectron spectroscopy.

The projected band structure of the siliborophene (Fig. 9) on ZrB_2(0001) shows a band crossing feature at the $\overline{\text{K}}$ point and $E_f - 1.4$ eV. The band-crossing state is energetically buried in the DOS of the other bands. Therefore, it is not expected to contribute to the electron transport properties as it is. However, the Dirac-point-like band crossing structure at the $\overline{\text{K}}$ point is found in a Si_3B_6 stand-alone layer, which was additionally calculated to elucidate the siliborophene bare electronic property. Figure 10 exhibits the electronic bands and DOS for the siliborophene stand-alone structure identical to that on ZrB_2(0001) (the "as-is" model) and the structure-optimized one (the "relaxed" model). Whereas each band-energy difference between the as-is and the relaxed models varies depending on each band, most bands retain the dispersion feature and are also similar to those of the projected band structure in Fig. 9(a) with a certain energy shift. It is noteworthy that both stand-alone models show the band-crossing point at $\overline{\text{K}}$ about 1 eV above the Fermi level, which is energetically not overlapped with the other bands. The appearance of this 0-gap state in both the as-is and relaxed models suggests robustness of this feature against the small structural perturbation. As exhibited in the projected band structures in Fig. 10(c), the p_z orbital component (normal to the surface) has a greater contribution to the band-crossing feature than the other orbital components. Judging from sinking of the band-crossing point to $E_f - 1.4$ eV on ZrB_2(0001) as shown in Fig. 9(a), it seems to play an important role in siliborophene adhesion to the ZrB_2(0001) substrate. However, the band-crossing point found in the stand-alone Si_3B_6 structure can exhibit unusual electronic features associated with

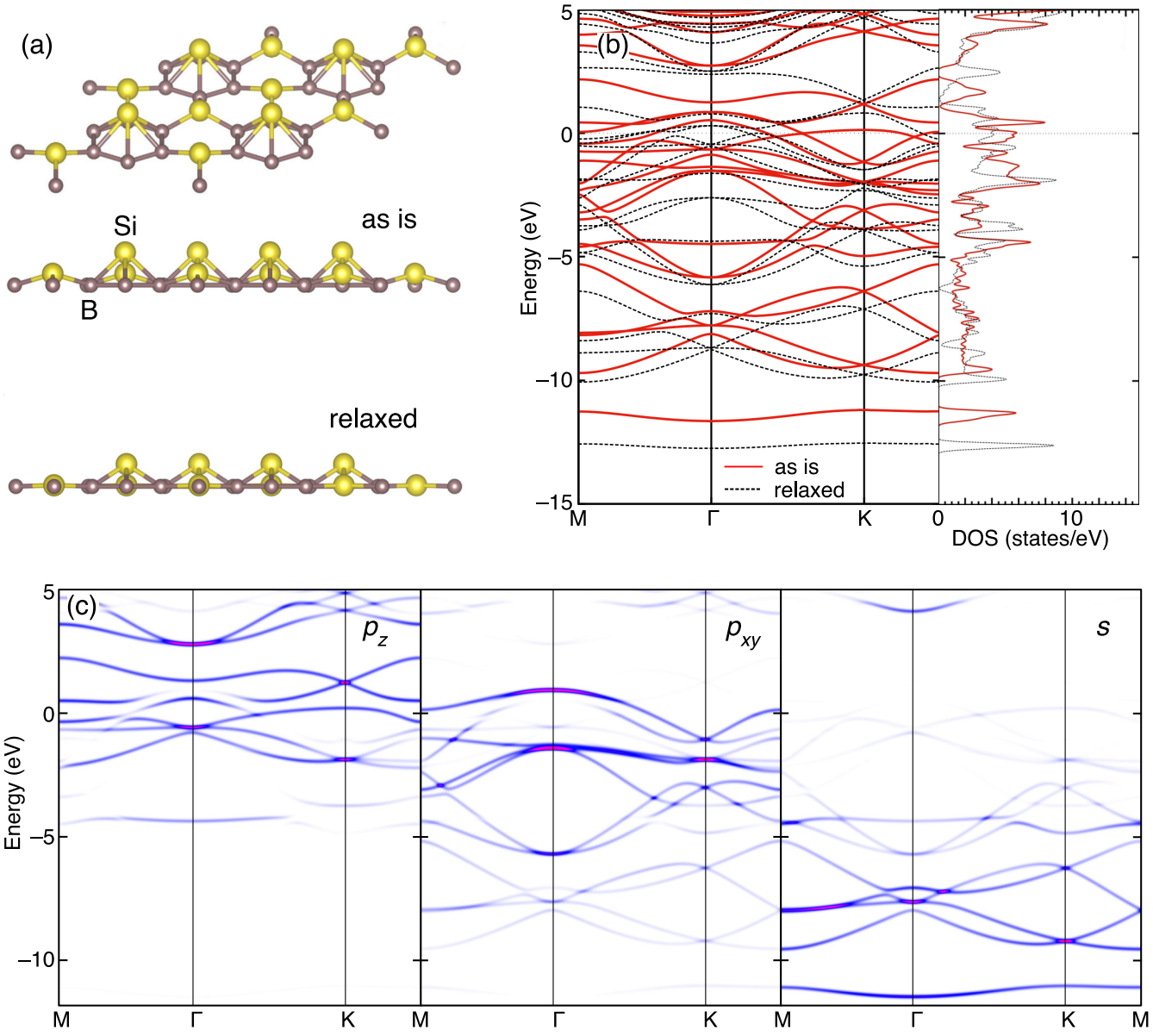

FIG. 10. Atomic and electronic structure for stand-alone Si_3B_6 siliborophene. (a) Bare siliborophene structure without the substrate (the as is model) was optimized in the periodic boundary condition. The final structure (the relaxed model) showed shorter Si-B bond length. The capping Si-B, bridging Si-B, and B-B bond lengths for as is (relaxed) model are, respectively, 222 (197), 199 (193), and 173 (173) pm. (b) All bands and DOS for the as is and relaxed models are plotted with red and dotted lines, respectively. (c) The projected bands of the as is model for the p_z, p_{xy}, and s orbital components. The Fermi level (E_f) is taken to be zero eV.

high-symmetric $\boldsymbol{k}$ points [1,2]. We expect that Fermi-level engineering, such as a simple different substrate adaptation and/or substitution of some atoms in the siliborophene layer, must contribute to its application in the near future.

IV. SUMMARY

This study explored characteristics of Si-B 2D compound on a $ZrB_2(0001)$ surface both experimentally and theoretically. Controlled adsorption of B onto a silicene-covered ZrB_2 at 1200 K realizes a 2×2 periodic Si_xB_y phase. This phase appeared to be very stable: no melting or phase transition was observed up to 1300 K until Si was desorbed. The phonon dispersion relations of this Si_xB_y phase were measured using HREELS.

To seek possible structures under a given composition in the 2×2 periodicity, SAMD calculations were done independently. The obtained structures were selected by comparing the calculated phonon with the experimentally obtained one. Among the many models calculated, only the Si_3B_6 siliborophene structure reproduced the experimentally obtained phonon dispersion well. Results suggest that this siliborophene is stable in view of the formation energy and the electronic band structure. In the electronic band structure of the siliborophene, several crossing bands are found at the $\overline{\mathrm{K}}$ point, which might make this material available in some applications with the use of Fermi-level engineering.

[1] A. K. Geim and K. S. Novoselov, Nat. Mater. **6**, 183 (2007).

[2] A. J. Mannix, B. Kiraly, M. C. Hersam, and N. P. Guisinger, Nat. Rev. Chem. **1**, 0014 (2017).

[3] T. Aizawa, R. Souda, S. Otani, Y. Ishizawa, and C. Oshima, Phys. Rev. B **42**, 11469 (1990).

[4] M. Alfano, C. Lamuta, G. Chiarello, and A. Politano, in *GraphITA* (Springer, Cham, 2017), pp. 47–59.

[5] T. Aizawa, S. Suehara, and S. Otani, J. Phys. Chem. C **118**, 23049 (2014).

[6] T. Aizawa, S. Suehara, and S. Otani, J. Phys.: Condens. Matter **27**, 305002 (2015).

[7] S. T. Oyama, *The Chemistry of Transition Metal Carbides and Nitrides* (Springer, Dordrecht, 1996), pp. 1–27.

[8] T. Lundström, in *Boron and Refractory Borides*, edited by V. I. Markovich (Springer, Berlin, 1977), pp. 351–376.

[9] S. Cahangirov, M. Topsakal, E. Aktürk, H. Şahin, and S. Ciraci, Phys. Rev. Lett. **102**, 236804 (2009).

[10] Y. C. Cheng, Z. Y. Zhu, and U. Schwingenschlögl, Europhys. Lett. **95**, 17005 (2011).

[11] L. Pan, H. J. Liu, Y. W. Wen, X. J. Tan, H. Y. Lv, J. Shi, and X. F. Tang, Phys. Lett. A **375**, 614 (2011).

[12] A. Fleurence, R. Friedlein, T. Ozaki, H. Kawai, Y. Wang, and Y. Yamada-Takamura, Phys. Rev. Lett. **108**, 245501 (2012).

[13] Y. Yamada-Takamura and R. Friedlein, Sci. Technol. Adv. Mater. **15**, 064404 (2014).

[14] R. Friedlein and Y. Yamada-Takamura, J. Phys.: Condens. Matter **27**, 203201 (2015).

[15] C.-C. Lee, A. Fleurence, Y. Yamada-Takamura, T. Ozaki, and R. Friedlein, Phys. Rev. B **90**, 075422 (2014).

[16] H. Van Bui, F. B. Wiggers, R. Friedlein, Y. Yamada-Takamura, A. Y. Kovalgin, and M. P. de Jong, J. Chem. Phys. **142**, 064702 (2015).

[17] F. B. Wiggers, Y. Yamada-Takamura, A. Y. Kovalgin, and M. P. de Jong, J. Chem. Phys. **147**, 064701 (2017).

[18] F. B. Wiggers, Y. Yamada-Takamura, A. Y. Kovalgin, and M. P. de Jong, Appl. Surf. Sci. **428**, 793 (2018).

[19] A. J. Mannix, X.-F. Zhou, B. Kiraly, J. D. Wood, D. Alducin, B. D. Myers, X. Liu, B. L. Fisher, U. Santiago, J. R. Guest, M. J. Yacaman, A. Ponce, A. R. Oganov, M. C. Hersam, and N. P. Guisinger, Science **350**, 1513 (2015).

[20] B. Feng, J. Zhang, Q. Zhong, W. Li, S. Li, H. Li, P. Cheng, S. Meng, L. Chen, and K. Wu, Nat. Chem. **8**, 563 (2016).

[21] B. Feng, J. Zhang, R.-Y. Liu, T. Iimori, C. Lian, H. Li, L. Chen, K. Wu, S. Meng, F. Komori, and I. Matsuda, Phys. Rev. B **94**, 041408 (2016).

[22] W. Li, L. Kong, C. Chen, J. Gou, S. Sheng, W. Zhang, H. Li, L. Chen, P. Cheng, and K. Wu, Sci. Bull. **63**, 282 (2018).

[23] T. Aizawa, W. Hayami, and S. Otani, Phys. Rev. B **65**, 024303 (2001).

[24] H. Kawanowa, R. Souda, S. Otani, and Y. Gotoh, Phys. Rev. Lett. **81**, 2264 (1998).

[25] H. Kawanowa, Y. Gotoh, S. Otani, and R. Souda, Surf. Sci. **433–435**, 661 (1999).

[26] T. Aizawa, S. Suehara, S. Hishita, and S. Otani, J. Phys.: Condens. Matter **20**, 265006 (2008).

[27] S. Suehara, T. Aizawa, and T. Sasaki, Phys. Rev. B **81**, 085423 (2010).

[28] Y. Ding and Y. Wang, J. Phys. Chem. C **117**, 18266 (2013).

[29] X. Tan, F. Li, and Z. Chen, J. Phys. Chem. C **118**, 25825 (2014).

[30] A. Hansson, F. de Brito Mota, and R. Rivelino, Phys. Rev. B **86**, 195416 (2012).

[31] H. Ibach and D. L. Mills, *Electron Energy Loss Spectroscopy and Surface Vibrations* (Academic Press, New York, 1982), p. 257.

[32] S. Otani and Y. Ishizawa, J. Cryst. Growth **165**, 319 (1996).

[33] P. Giannozzi, S. Baroni, N. Bonini, M. Calandra, R. Car, C. Cavazzoni, D. Ceresoli, G. L. Chiarotti, M. Cococcioni, I. Dabo, A. Dal Corso, S. de Gironcoli, S. Fabris, G. Fratesi, R. Gebauer, U. Gerstmann, C. Gougoussis, A. Kokalj, M. Lazzeri, L. Martin-Samos *et al.*, J. Phys.: Condens. Matter **21**, 395502 (2009).

[34] P. Giannozzi, O. Andreussi, T. Brumme, O. Bunau, M. Buongiorno Nardelli, M. Calandra, R. Car, C. Cavazzoni, D. Ceresoli, M. Cococcioni, N. Colonna, I. Carnimeo, A. Dal Corso, S. de Gironcoli, P. Delugas, R. A. DiStasio, A. Ferretti, A. Floris, G. Fratesi, G. Fugallo *et al.*, J. Phys.: Condens. Matter **29**, 465901 (2017).

[35] J. P. Perdew, K. Burke, and M. Ernzerhof, Phys. Rev. Lett. **77**, 3865 (1996).

[36] K. F. Garrity, J. W. Bennett, K. M. Rabe, and D. Vanderbilt, Comput. Mater. Sci. **81**, 446 (2014).

[37] See Supplemental Material at http://link.aps.org/supplemental/10.1103/PhysRevMaterials.3.014005 for the effect of van der Waals interaction and the detailed atomic coordinates.

[38] H. J. C. Berendsen, J. P. M. Postma, W. F. van Gunsteren, A. DiNola, and J. R. Haak, J. Chem. Phys. **81**, 3684 (1984).

[39] W. Humphrey, A. Dalke, and K. Schulten, J. Mol. Graphics **14**, 33 (1996).

[40] K. Momma and F. Izumi, J. Appl. Crystallogr. **41**, 653 (2008).

[41] D. Sanchez-Portal, E. Artacho, and J. M. Soler, Solid State Commun. **95**, 685 (1995).

[42] P.-O. Löwdin, Adv. Quantum Chem. **5**, 185 (1970).

[43] G. Kresse and J. Furthmüller, Comput. Mater. Sci. **6**, 15 (1996).

[44] T. Aizawa, S. Suehara, S. Hishita, S. Otani, and M. Arai, Phys. Rev. B **71**, 165405 (2005).